Applied Catalysis B: Environmental 138–139 (2013) 191–198

Contents lists available at SciVerse ScienceDirect

Applied Catalysis B: Environmental

journal homepage: www.elsevier.com/locate/apcatb

Insights into the role of SO_2 and H_2O on the surface characteristics and de-N_2O efficiency of Pd/Al_2O_3 catalysts during N_2O decomposition in the presence of CH_4 and O_2 excess

M. Konsolakis[a,*], I.V. Yentekakis[a], G. Pekridis[b], N. Kaklidis[b], A.C. Psarras[c], G.E. Marnellos[b,c]

[a] Laboratory of Physical Chemistry and Chemical Processes, Department of Sciences, Technical University of Crete, GR-73100 Chania, Crete, Greece
[b] Department of Mechanical Engineering, University of Western Macedonia, Bakola & Sialvera, GR-50100 Kozani, Greece
[c] Chemical Process Engineering Research Institute, Centre for Research & Technology Hellas, 6th km. Charilaou – Thermi Rd., P.O. Box 60361, GR-57001 Thermi, Thessaloniki, Greece

ARTICLE INFO

Article history:
Received 7 December 2012
Received in revised form 11 February 2013
Accepted 18 February 2013
Available online 26 February 2013

Keywords:
N_2O decomposition
Palladium
CH_4
SO_2
H_2O
XPS
DRIFTS
FTIR-pyridine

ABSTRACT

The catalytic abatement of nitrous oxide (N_2O), a powerful greenhouse and ozone depletion gas, is an efficient end-of-pipe technology for N_2O emissions control. However, de-N_2O performance is notably suppressed by SO_2 and H_2O presence on the flue gases, whereas little is known about their influence on catalyst surface chemistry. In the present study, the impact of sulfur dioxide and water vapor on the catalytic performance of Pd/Al_2O_3 catalysts during the N_2O decomposition in the presence of CH_4 and O_2 excess is investigated, with particular emphasis on the corresponding surface chemistry modifications. Catalytic activity and stability measurements, in conjunction with a kinetic study, were carried out to elucidate the individual effect of each molecule on de-N_2O performance. X-ray photoelectron spectroscopy (XPS), diffuse reflectance infrared Fourier transform spectroscopy (DRIFTS) and Fourier transform infrared spectroscopy (FTIR) of pyridine adsorption are employed to evaluate the impact of SO_2 and H_2O molecules on catalyst surface chemistry, which is appropriately correlated with the achieved catalytic performance. The results revealed that the de-N_2O efficiency can be substantially improved by CH_4 under reducing (absence of O_2) conditions, due to the scavenging of strongly adsorbed O_{ads} species by the hydrocarbon; however, under O_2 excess conditions the beneficial effect of CH_4 is marginal. Water vapor in the feed has a detrimental influence on both N_2O and CH_4 conversions, which, however, is totally reversible; the latter is mainly ascribed to the competitive adsorption of H_2O molecules on catalyst surface. In contrast, SO_2 addition in feed stream results in a severe, irreversible deactivation; SO_2 leads to the creation of Brönsted acid sites on Al_2O_3 support, which in turn results in highly oxidized Pd entities, inactive for N_2O decomposition.

1. Introduction

Nitrous oxide (N_2O) has recently attracted great attention, due to its environmental impact. It is a powerful greenhouse gas with a global warming potential (GWP) about 300 times higher than that of CO_2, while at the same time it notably contributes to stratospheric ozone depletion [1–3]; lately published articles reveal the dominant input of N_2O on the world climate and ozone layer destruction [4,5].

Nowadays, N_2O atmospheric concentration is increasing at a rate of 0.5–1.0 ppbv per year as a consequence of anthropogenic activities, including mainly the combustion of fossil fuels and biomass, the use of fertilizers in land cultivation, the production of adipic and nitric acid in chemical plants and the deNOx processes [1]. Therefore, the control of N_2O emissions from combustion and chemical processes, in which end-of-pipe technologies can be effectively applied, is of significant importance toward the N_2O abatement. In recognition of the above aspects, extended efforts have been recently devoted to N_2O abatement by different remediation methods such as thermal decomposition, selective adsorption, plasma technology, catalytic decomposition and selective catalytic reduction (SCR) of N_2O with various reducing agents. Among them, the catalytic technologies represent the most promising choices due to their lower energy requirements and consequently lower cost.

Up to date, various catalysts such as supported noble metals [6–11], metal oxides [12,13], spinels [14,15], zeolites [16,17], perovskites [18,19] and hydrotalcites [20,21] have been

* Corresponding author. Tel.: +30 28210 37682; fax: +30 28210 37843.
E-mail address: mkonsol@science.tuc.gr (M. Konsolakis).

0926-3373/$ – see front matter © 2013 Elsevier B.V. All rights reserved.
http://dx.doi.org/10.1016/j.apcatb.2013.02.038

investigated for N_2O direct decomposition. However, in most cases strongly adsorbed atomic oxygen originating either from gas phase oxygen or from N_2O decomposition causes poisoning of catalysts active centers; this is the main inhibiting factor in catalytic de-N_2O processes [1–3]. To this end, the catalytic decomposition of N_2O in the presence of different reducing agents, such as CO and HCs, represents a promising technology for N_2O abatement, since the presence of a reductant can facilitate the removal of strongly adsorbed oxygen atoms [3,22–24]. In addition, from the environmental point of view, it is of great interest to study the N_2O decomposition in the presence of CO or HCs, which can lead to the simultaneous abatement of two pollutants [16,23,24]. Taking into account the co-existence of methane in the off-gases of fossil fuels combustion processes (especially those employing natural gas as a fuel) as well as its significant greenhouse potential, it is of particular interest to investigate the de-N_2O process in the presence of CH_4.

In our previous study concerning the effect of metal (M) entity (M: Pd, Rh, Ru, Cu, Fe, In and Ni) and reducing agents (CO, CH_4 or C_3H_8) on N_2O decomposition over M/Al_2O_3 supported catalysts, it was found that Pd/Al_2O_3 is among the most active catalysts for the simultaneous abatement of CH_4 and N_2O [10]. However, the co-existence of other gases inevitably present in the flue gas stream, such as SO_2 and H_2O, significantly suppresses the catalytic performance thus limiting the catalyst's applicability [10]. On the same basis, a notable inhibition of de-N_2O performance was observed over the highly active Rh and Ru based catalysts, when SO_2 or H_2O were added to the feed [8,9]. In accordance to authors the deactivation caused by H_2O is to a great extent reversible without affecting catalyst properties. On the other hand, a considerable permanent decrease in activity is caused by SO_2 [8,9].

Although the deactivation of supported metal catalysts by SO_2 is a well known phenomenon, there still exists an extended discrepancy in the literature concerning the mechanism of this deactivation. According to some authors, the deactivation induced by SO_2 can be mainly ascribed to the formation of inactive metal–SO*x* species [*e.g.*, 25]. On the other hand, several studies over metal supported catalysts on sulfating (like Al_2O_3) supports reveal that the deactivation should be primarily assigned to the sulfation of support [*e.g.*, 26]. Toward this direction, the present study aims to gain further insight into the precise mechanism of action of SO_2 during the de-N_2O process.

Based on the above aspects, the objective of this work is to gain insight into the effect of SO_2 and H_2O on the activity of Pd/Al_2O_3 catalysts during the N_2O abatement from combustion processes effluents, with particular emphasis on the surface chemistry modifications induced by SO_2 and H_2O. To this end, activity and stability measurements are combined with kinetic and surface analysis data obtained by XPS, DRIFTS and FTIR-pyridine adsorption, to attain the closest relationship between the catalysts surface characteristics and the corresponding de-N_2O efficiency.

2. Experimental

2.1. Catalyst preparation and characterization

The dry impregnation method was used in order to synthesize $Pd/\gamma\text{-}Al_2O_3$ catalysts with a nominal Pd loading of 2.0 wt%, using $\gamma\text{-}Al_2O_3$ carrier (Engelhard, 180–355 μm) and a $Pd(NO_3)_2{\cdot}3H_2O$ solution (Alpha Products) as precursors. Following impregnation, the catalyst was dried at 120 °C for 2 h and calcined at 600 °C for 4 h, under stagnant air; catalyst obtained by this procedure is hereinafter referred as "fresh" catalyst. The BET surface area of the as prepared catalyst was determined by Nitrogen physical adsorption/desorption experiments at −196 °C using an Autosorb-1 (Quantachrome) flow apparatus and was found to be 173 m^2/g. For accurate metal loading determination, the inductively coupled plasma atomic emission spectroscopy (ICP/AES) was used, resulting in a Pd loading of 2.078 ± 0.075 wt%.

2.2. Catalytic performance measurements

Catalytic experiments were carried out in a U-shape quartz fixed-bed reactor (0.8 cm, i.d.) loaded with 150 mg of catalyst. The total gas flow rate during catalytic measurements was kept constant at 120 cm^3/min, corresponding to W/F and GHSV values of 0.075 g s/cm^3 and 35,000 h^{-1}, respectively. The typical feed composition employed during catalytic tests was 0.12% N_2O, 5% O_2, 0.5% CH_4, 0–300 ppm SO_2, 0–3% H_2O balanced with He. Water was introduced into reactor by bubbling the reactants mixture through a saturator. Reactants and products analysis was performed by on-line gas chromatography (SHIMADZU 14B) equipped with a molecular sieve 13X column for oxygen, nitrogen, methane and carbon monoxide separation and a porapak QS column for nitrous oxide and carbon dioxide separation. Prior to each experiment, catalysts were heated in He flow (600 °C/1 h/100 cm^3 min^{-1}) in order to eliminate possible residue from the metal precursor and to ensure stable operation. Besides typical *light-off* performance measurements, where N_2O and CH_4 conversions were recorded as a function of temperature in the interval of 100–600 °C, intrinsic kinetic data were also acquired. In the latter case attention was given to the reactants conversions: they were kept less than 15% to eliminate mass and heat transfer limitations. Apparent activation energies were determined in the temperature interval of 280–380 °C, by employing the following standard reactants concentrations: N_2O (0.12%), O_2 (5%), CH_4 (0.5%), H_2O (3%), SO_2 (0.01%). Apparent partial reaction orders in respect to all reactants (N_2O, O_2, CH_4, H_2O, SO_2) were also estimated by varying reactants concentration, at constant temperature, as follows: N_2O (0.04–0.2%), O_2 (1.5–8.5%), CH_4 (0.2–1.65%), H_2O (1–3%), SO_2 (0.05–0.4%).

2.3. XPS characterization

The impact of SO_2 and H_2O on Pd chemical state and surface elemental composition was investigated by means of X ray photoelectron spectroscopy (XPS) over Pd/Al_2O_3 catalysts pretreated either in SO_2- or H_2O-containing reaction mixtures. Photoelectron spectra were recorded over samples in the form of pellets (1 mm × 10 mm) in an ultra high vacuum system (UHV), consisting of a fast entry specimen assembly, a sample preparation and an analysis chamber. The base pressure in both chambers was 1×10^{-9} mbar. Non-monochromatized Mg Kα line at 1253.6 eV and an analyzer pass energy of 97 eV, giving a full width at half maximum (FWHM) of 1.7 eV for the Au $4f_{7/2}$ peak, were used. Using a fitting routine, XPS core level spectra were resolved into their Gaussian and Lorentzian components, after a Shirley background subtraction. The C1s peak at 284.6 eV was used for binding energy (BE) scale calibration.

2.4. In situ DRIFTS studies

Diffuse reflectance IR spectra were collected using a NICOLET 6700 spectrometer, equipped with a MCT/B detector and an IR cell loaded with ~50 mg of catalyst. Infrared spectra were obtained with resolution of 4 cm^{-1} and accumulation of 64 scans. Pretreatment procedure before spectra acquisition has as follows: (i) heating to 500 °C under He flow for 30 min, (ii) oxidation at 500 °C with 20% O_2 for 30 min (iii) purging with He at 500 °C for 30 min, (iv) background spectra acquisition at the desired temperatures under He flow.

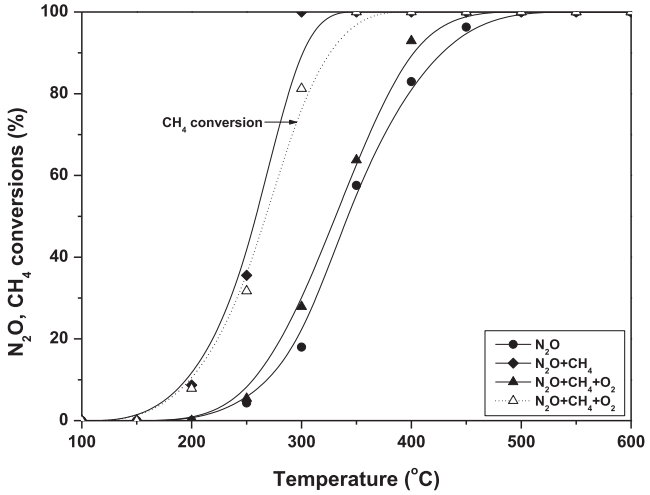

Fig. 1. Effect of feed composition on N_2O and CH_4 conversion profiles over Pd/Al_2O_3 catalysts. Reaction conditions: 0.12% N_2O, 0.5% CH_4, 5% O_2 in He; total flow rate = 120 cm^3/min; catalyst weight = 0.15 g.

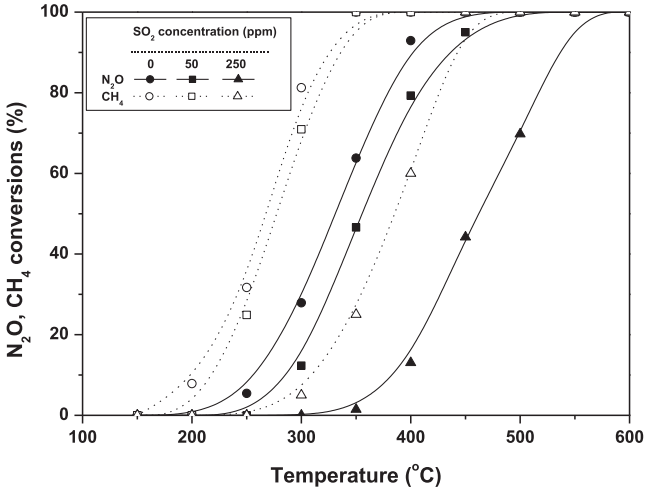

Fig. 2. Effect of SO_2 concentration on N_2O and CH_4 conversion profiles over Pd/Al_2O_3 catalysts. Reaction conditions: 0.12% N_2O, 0.5% CH_4, 5% O_2 in He; total flow rate = 120 cm^3/min; catalyst weight = 0.15 g.

Two different set of DRIFTS experiments were performed:

(i) Steady-state experiments, employing CO (0.5% in He) as a probe molecule, over fresh and pre-sulfated catalysts to investigate the permanent effect of SO_2 on the catalyst's chemisorptive properties.
(ii) Transient experiment of CO adsorption involving at first catalyst exposure to CO and then switch to CO + H_2O mixture in order to *in situ* investigate the effect of H_2O on the nature and relative population of pre-adsorbed species. The corresponding experiment with SO_2 was not performed to avoid any damage effect of SO_2 on IR cell.

2.5. FTIR studies of pyridine adsorption

Catalyst acidic properties were evaluated by means of FTIR studies of pyridine adsorption. IR spectra were collected with a resolution of 4 cm^{-1}, using a Nicolet 5700 spectrometer equipped with a homemade stainless steel IR cell with CaF_2 windows. The infrared cell, loaded with self-supporting wafers (~15 mg/cm^2), is connected to a high vacuum line consisting of turbomolecular and diaphragm pumps; both sample holder and vacuum line are heated to avoid pyridine condensation. Before IR spectra acquisition, samples were heated at 450 °C under vacuum (10^{-6} mbar) for 1 h to desorb any physisorbed species. Then the reference spectrum of each sample is collected at 150 °C. Spectra of adsorbed pyridine were obtained at 150 °C at 1 mbar by equilibrating the catalyst wafer with the probe vapor, added in pulses for 1 h.

3. Results and discussion

3.1. Effect of CH_4 and O_2 on N_2O decomposition

Fig. 1 depicts the dependence of N_2O (and CH_4) conversion on reaction temperature (100–600 °C) over Pd/Al_2O_3 catalysts, for the direct N_2O decomposition and the $N_2O + CH_4$ reaction, either in the absence or in the presence of excess O_2. It is obvious that under reducing conditions (absence of O_2), CH_4 substantially improves the de-N_2O performance, shifting the N_2O conversion profile to notably lower temperatures. Particularly, the presence of CH_4 results in complete elimination of N_2O at temperatures as low as 300 °C, compared to 500 °C in the case of direct N_2O decomposition. However, at O_2 excess conditions the influence of CH_4 is marginal, resulting in an N_2O conversion profile slightly better than that obtained for N_2O direct decomposition. The latter indicates that a beneficial effect of CH_4 on N_2O decomposition can be obtained only in the absence of O_2. This behavior can be interpreted by considering the well established in the literature mechanism of N_2O decomposition [27], which involves N_2O dissociation to N_2 and O(ad) as the key step for N_2O elimination, even in the presence of a reducing agent. In this context, the promoting effect of CH_4 under reducing conditions is attributed to the "clean up" of catalyst surface from adsorbed oxygen species, which are blocking the active sites thus hindering the N_2O adsorption/decomposition. Under oxygen excess conditions, CH_4 consumption proceeds more rapidly compared to N_2O decomposition (Fig. 1, dotted line), thus limiting its scavenging effect.

3.2. Effect of SO_2 and H_2O on N_2O decomposition

Since combustion effluent gases inevitably contain H_2O and SO_2, it is of particular interest to investigate the influence of these molecules on de-N_2O performance and stability of Pd/Al_2O_3 catalysts. Fig. 2 presents both the N_2O and CH_4 conversions as a function of temperature at different SO_2 concentrations (0, 50 and 250 ppm) in the presence of excess O_2. It is obvious that SO_2 has a detrimental effect on both N_2O and CH_4 conversions, which is exacerbated upon increasing SO_2 concentration. In particular, addition of 50 ppm SO_2 in the feed stream results in an increase of N_2O and CH_4 *light-off* temperatures (*i.e.*, temperature for 50% conversion) by *ca.* 25 and 10 °C, respectively. This influence become even worse for higher levels of SO_2 in the feed; SO_2 concentration of 250 ppm results in a shift of N_2O and CH_4 conversion profiles by ~130 and ~120 °C to higher temperatures, respectively.

The corresponding results concerning the influence of H_2O are depicted in Fig. 3. It is evident that the de-N_2O performance is progressively suppressed by increasing H_2O content in the feed; the N_2O *light-off* temperature is increased by 45 and 85 °C, for 1.0% and 3.0% H_2O, respectively, in respect to 330 °C in the case of H_2O-free feed. An analogous inhibition is also observed in CH_4 conversion: the CH_4 *light-off* temperature of 267 °C corresponding to H_2O-free feed is shifted to 278 (ΔT = +11 °C) and 330 °C (ΔT = +63 °C), respectively, for 1% and 3% H_2O in the feed.

The response of de-N_2O efficiency in SO_2 and H_2O containing mixtures was also investigated through step-change experiments, where the N_2O conversion was continuously monitored for 8 h while the feed stream was periodically

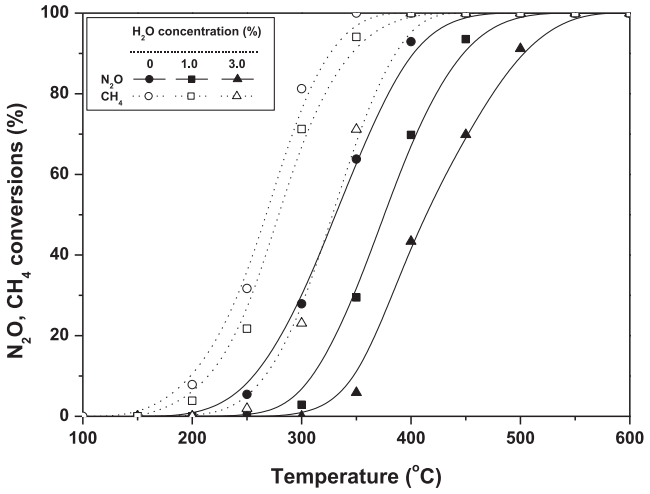

Fig. 3. Effect of H_2O concentration on N_2O and CH_4 conversion profiles over Pd/Al_2O_3 catalysts. Reaction conditions: 0.12% N_2O, 0.5% CH_4, 5% O_2 in He; total flow rate = 120 cm^3/min; catalyst weight = 0.15 g.

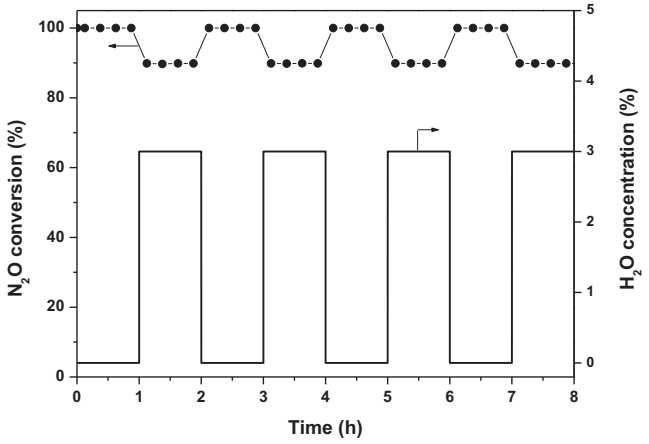

Fig. 5. Response of N_2O conversion to step changes of H_2O concentration over Pd/Al_2O_3 catalysts. Reaction conditions: 0.12% N_2O, 0.5% CH_4, 5% O_2 in He; total flow rate = 120 cm^3/min; catalyst weight = 0.15 g; T = 480 °C.

switched from SO_2 (or H_2O) free mixtures to SO_2 (or H_2O) containing mixtures. Fig. 4 depicts the response of N_2O conversion to step changes of SO_2 concentration (0–300 ppm) at 480 °C. In the first step (t = 0–1 h), when the catalyst was exposed to SO_2-free mixture, the recorded N_2O conversion is stable and equal to 100%. However, addition of 50 ppm SO_2 in feed (t = 1–2 h), results in a gradual deactivation; after 1 h of exposure to 50 ppm SO_2 the N_2O conversion has been steadily decreased to a value of 88%. In the next SO_2-containing step (t = 3–4 h; [SO_2] = 100 ppm) a rapid decrease of N_2O conversion from 88% to 33% is observed, indicating that the deactivation induced by SO_2 depends strongly both on the exposure time and SO_2 concentration. A further decrease in N_2O conversion values to 23% and 16%, respectively, is finally recorded during the 150 and 300 ppm SO_2-containing steps (t = 5–6 h and t = 7–8 h, respectively). It is worth emphasizing that during the SO_2 -free steps (*i.e.*, t = 2–3 h, 4–5 h, and 6–7 h) only a slight restoration of the catalytic activity is taking place, implying the irreversible nature of SO_2 poisoning.

The corresponding results concerning the response of N_2O conversion on periodic step changes of H_2O-addition in the feed is depicted in Fig. 5. Introduction of 3% H_2O causes a sudden (step) drop on the N_2O conversion, from 100% to ~90%. By removing H_2O the de-N_2O performance is totally recovered. This is repeated in all four cycles involved in the experiment (Fig. 5), indicating that H_2O, in contrast to SO_2, has a completely reversible detrimental effect on de-N_2O catalytic performance.

The impact of H_2O and SO_2 on the durability of Pd/Al_2O_3 catalysts was also investigated in long-term stability tests (12 h) under SO_2- or H_2O-containing feeds. Fig. 6 illustrates the N_2O conversion as a function of time during the N_2O reduction by CH_4 under O_2 excess conditions, either in the presence or in the absence of SO_2 or H_2O. It is obvious that in the absence of SO_2 and H_2O the N_2O conversion remains constant and equal to 100% over the whole time period investigated, implying the excellent stability of Pd/Al_2O_3 catalysts under these reaction conditions. However, in the presence of 3% H_2O in the feed stream, the N_2O conversion drops in the first 1 h to ~90%, remaining then constant for the rest of the time. Addition of 150 ppm SO_2 in the feed stream leads in a progressive deactivation, with a characteristic rapid initial progress; in the first 6 h the N_2O conversion is dropped by ~80 percentage units (from 100% to ~20%), whereas during the next 6 h a further drop by only 10 additional percentage units occurred.

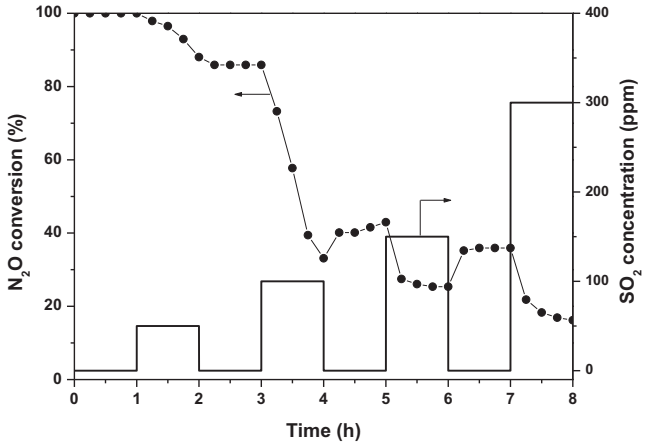

Fig. 4. Response of N_2O conversion to step changes of SO_2 concentration over Pd/Al_2O_3 catalysts. Reaction conditions: 0.12% N_2O, 0.5% CH_4, 5% O_2 in He; total flow rate = 120 cm^3/min; catalyst weight = 0.15 g; T = 480 °C.

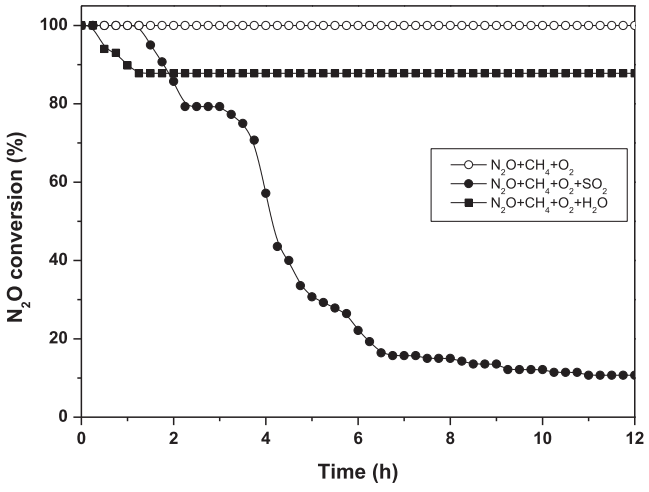

Fig. 6. Response of N_2O conversion to long-term stability tests carried out in the absence or presence of SO_2 (or H_2O) in reaction feed stream over Pd/Al_2O_3 catalysts. Reaction conditions: 0.12% N_2O, 0.5% CH_4, 5% O_2, 0.015% SO_2, 3% H_2O in He; total flow rate = 120 cm^3/min; catalyst weight = 0.15 g; T = 480 °C.

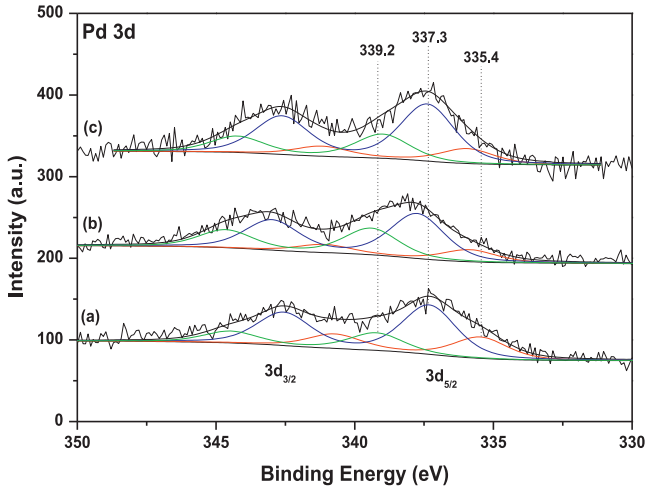

Fig. 7. Pd 3d XP spectra of Pd/Al_2O_3 catalysts exposed to different pretreatment: fresh (a), SO_2-treated (b) and H_2O-treated catalysts (c). Pretreatment was carried out at 480 °C for 8 h in 0.12% N_2O + 0.5% CH_4 + 5% O_2 reaction mixture containing either 0.015% SO_2 (SO_2-treated catalysts) or 3% H_2O (H_2O-treated catalysts).

3.3. XPS studies

To determine the effect of SO_2 and H_2O on Pd chemical state and surface composition, XPS studies were carried out over Pd/Al_2O_3 samples exposed to different pretreatment. The samples were pretreated at 480 °C for 8 h in a reaction mixture ($N_2O + CH_4 + O_2$) containing either 3% H_2O (H_2O-treated catalysts) or 150 ppm SO_2 (SO_2-treated catalysts). Fig. 7 depicts the spectral region of Pd $3d_{5/2}$ and $3d_{3/2}$ doublets over fresh (spectrum a), SO_2-treated (spectrum b) and H_2O-treated (spectrum c) Pd/Al_2O_3 catalysts. Spectra deconvolution reveals three individual components, showing the distribution of binding energies in the Pd 3d spectra region. The spectrum of fresh catalyst (spectrum a) is characterized by Pd $3d_{5/2}$ binding energies at 335.4, 337.3 and 339.2 eV (Fig. 7 and Table 1). The first state is assigned to metallic Pd (Pd^0), the second to oxidized Pd (PdO_x, $x \geq 1$) and the third to highly oxidized Pd (PdO_x, $x \geq 2$) [28–30]. The relative amounts of palladium states, calculated from the areas of the fitted Gaussian–Lorentzian components of Pd 3d envelope (Table 1), indicate that the majority of Pd species lie in an oxidized state, in consistency with the pretreatment procedure. Focusing now on the spectrum of SO_2-treated catalyst (Fig. 7, spectrum b) it is obvious that significant modifications have been induced on the Pd chemical state, which can be summarized as follows:

(i) a shift of Pd 3d peaks to higher binding energies is attained (Fig. 7 and Table 1). On sulfated catalysts the majority of palladium entities (86%) are located at BE higher than 337.8 eV, corresponding to highly oxidized Pd species, whereas a small portion (14%) lies on BE of 335.9 eV. The value of 335.9 eV is too high for metallic Pd^0, possibly implying an intermediate chemical state between reduced and oxidized Pd species.

(ii) a decrease of the relative amount of Pd^0 species is obtained over sulfated catalysts; the portion of Pd entities that lie in reduced state decreased from 24% over fresh catalyst to values lower than 14% over SO_2-treated catalyst (Table 1).

Based on the above aspects it can be deduced that SO_2 addition in the feed results in the formation of highly oxidized Pd species. These species are considered to be inactive for de-N_2O process, given that SO_2-treated catalysts are ineffective for N_2O decomposition (Fig. 6). In a similar manner, the deactivation observed by Corro et al. [31] during methane oxidation in the presence of SO_2 over Pd/Al_2O_3 catalysts, has been ascribed to the formation of sulfate species, which lead to an increase of Pd-O bond energy and therefore to limited oxidation activity.

It is also worth emphasizing that catalyst pretreatment with a SO_2 containing reaction mixture leads to an increase of Pd/Al atomic ratio (Table 1), implying no significant tendency for sulfur species accumulation over Pd surface. The latter is in accordance with the tendency of Al_2O_3 support to act as sulfur compounds sink [26] and is further verified by DRIFTS data presented below.

Comparison of the spectra of H_2O-treated and fresh catalysts (Fig. 7, spectra c and a, respectively) reveals that H_2O pretreatment, results in much lower modifications in Pd 3d envelope, compared to those imposed by SO_2-pretreatment; although the shape of Pd 3d envelope is changed upon H_2O pretreatment, the distribution of binding energies in Pd 3d region remains unaffected. In addition, the Pd/Al ratio remains constant upon H_2O pretreatment (Table 1) implying no changes of Pd distribution over the Al_2O_3 support. Taking into account that XPS spectra were carried out over *ex situ* H_2O-treated catalysts, it can be deducted that the presence of H_2O in the feed stream does not result in any permanent changes on catalysts surface characteristics. To this end, the inhibiting effect of H_2O (Fig. 5) may be ascribed to the *in situ* poisoning of catalyst surface by adsorbed hydroxyl groups that compete for the same active sites with N_2O and CH_4 reactants. The latter is fully confirmed below by *in situ* DRIFTS data concerning the impact of H_2O on the chemisorptive properties of Pd/Al_2O_3 catalyst.

3.4. DRIFTS studies

To further elucidate the influence of H_2O and SO_2 on catalyst surface chemistry, *in situ* DRIFTS studies were undertaken using CO as a probe molecule. This approach allows to gain *in situ* insight, under real working conditions, into the nature and the chemical state of surface sites.

Fig. 8 depicts the spectra of adsorbed species obtained in the C—O stretching frequency region (2200–1800 cm^{-1}) over fresh and SO_2-treated Pd/Al_2O_3 catalysts following CO adsorption at 25 °C and then purging with He to remove the gas phase and weakly adsorbed species. The spectrum of fresh catalyst (spectrum a) is characterized by a well resolved band at 2096 cm^{-1} and two overlapping bands at 1966 and 1922 cm^{-1}. These bands are in agreement with those reported previously for Pd–CO interaction [11,32,33]. The band at 2096 cm^{-1} is ascribed to CO species linearly bonded to reduced Pd sites (Pd^0–CO complexes). The bands at 1966 and 1922 cm^{-1} can be attributed to bridged bonded CO on Pd sites; the band at 1966 cm^{-1} is usually ascribed to isolated $(Pd^0)_2$–CO complexes formed on Pd

Table 1
Binding energies of core electrons and surface atomic ratios of Pd/Al_2O_3 catalysts exposed to different pretreatment (values in parenthesis referred to peak percentage).

Catalyst sample	Binding energies (eV) of Pd $3d_{5/2}$			Surface atomic ratios	
				Pd/Al	S/Al
Fresh	335.4 (24)	337.3 (56)	339.2 (20)	0.025	–
SO_2-treated	335.9 (14)	337.8 (54)	339.4 (32)	0.030	0.050
H_2O-treated	335.9 (17)	337.4 (59)	339.0 (24)	0.025	–

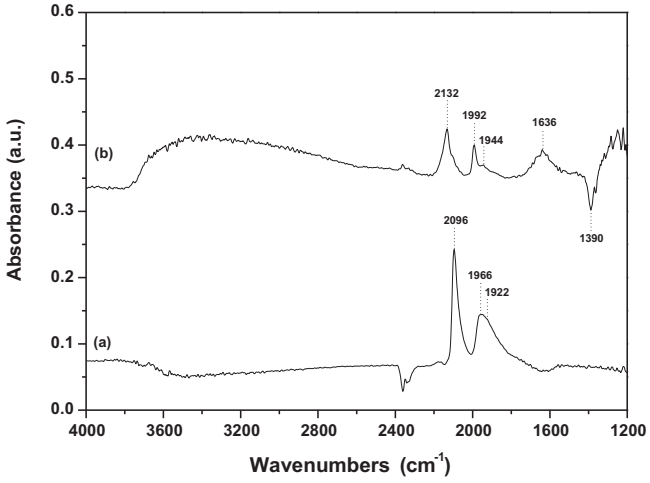

Fig. 8. DRIFTS spectra of CO adsorption at 25 °C over fresh (a) and SO_2-treated (b) Pd/Al_2O_3 catalysts. IR chamber feed: 0.5% CO in He; total flow rate = 80 cm^3/min. Pretreatment conditions as in Fig. 7.

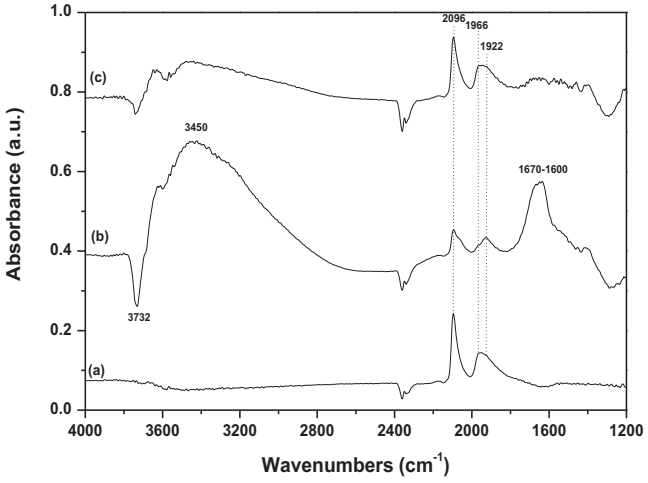

Fig. 10. DRIFTS spectra of CO adsorption at 25 °C over Pd/Al_2O_3 catalysts, obtained: before H_2O introduction (a), during CO + H_2O co-adsorption (b) after H_2O removal from feed stream (c). IR chamber feed: 0.5% CO, 3% H_2O in He; total flow rate = 80 cm^3/min.

(1 0 0) or (1 1 0) planes, whereas the band at 1922 cm^{-1} to bridged carbonyls on Pd (1 1 1) planes [11,32,33].

Focusing now on the corresponding spectrum of SO_2-treated catalyst (spectrum b), it is obvious that significant modifications on surface behavior have been induced by SO_2 pretreatment. These modifications include (i) an intensity decrease of CO adsorbed species, (ii) a notable blue shift of *ca.* 36 and 25 cm^{-1} for linearly and bridged bonded CO species, respectively, and (iii) the appearance of a negative band at 1390 cm^{-1}, characteristic of sulfate species on Al_2O_3 [26,34,35]. In addition a band at *ca.* 1636 cm^{-1} is appeared over SO_2-treated catalysts which can be assigned to the bending vibration of adsorbed water molecules. Similar bands have been observed upon SO_2 or H_2S adsorption on Al_2O_3 supported catalysts [*e.g.*, 36]. These modifications can be mainly understood by taking into account the effect of sulfate species on Pd chemical state. Considering the electronegative nature of sulfate species the blue shift of carbonyls should be attributed to a strong electronic interaction between Pd sites and sulfates. Indeed, sulfur species are expected to decrease the electron density of the adjacent Pd sites through an electron attractor effect, thus hindering the back-donation from Pd entities to $2\pi^*$ antibonding orbitals of CO. This results in the strengthening of C—O bond, blue shifting its vibration to higher frequencies where Pd^+–CO interactions are expected. In line with this explanation the band at 2132 cm^{-1}, observed here over SO_2-treated catalysts, is usually attributed to CO species bonded on highly oxidized Pd sites [37,38], implying the significant influence of sulfates on Pd oxidation state. The latter is consistent with the formation of highly oxidized metal sites over sulfated catalysts [39].

The decrease in carbonyls intensity upon sulfation can be mainly interpreted on the basis of electronic and/or geometric influence of sulfate species on Pd sites. Electron acceptor compounds could substantially decrease the electron density of Pd sites, thus hindering the CO adsorption. In addition, SO_2 treatment could have resulted in the formation of sulfate species on Pd sites, leading to an inferior chemisorption ability of Pd/Al_2O_3 catalysts. However, taking into account the appearance of sulfur species on alumina phase (band at 1390 cm^{-1}) as well as the absence of any band ascribed to Pd–SO_2 interaction (*e.g.* at *ca.* 1435 cm^{-1}), it should be argued that Al_2O_3 support acts as a sulfate sink, partially preventing the sulfation of Pd sites. The latter is in agreement with the XPS results, which reveal that there is no significant tendency for sulfur species accumulation on Pd sites. Accordingly, it has been argued in the literature that SO_2 is firstly oxidized to SO_3 over Pd entities and then migrates to Al_2O_3 support forming $Al_2(SO_4)_3$ [26,36]. To this end the electronic modifications induced by SO_2 over Pd sites should be mainly attributed to metal–support interactions rather than to the direct interface of Pd with sulfur compounds. The latter is schematically illustrated in Fig. 9 which depicts the mechanism of action of SO_2 on de-N_2O process over Pd/Al_2O_3 catalysts.

The influence of H_2O on the surface behavior of Pd/Al_2O_3 catalyst was *in situ* investigated by flowing CO through a steam saturator and then monitoring the changes in CO spectra. Fig. 10

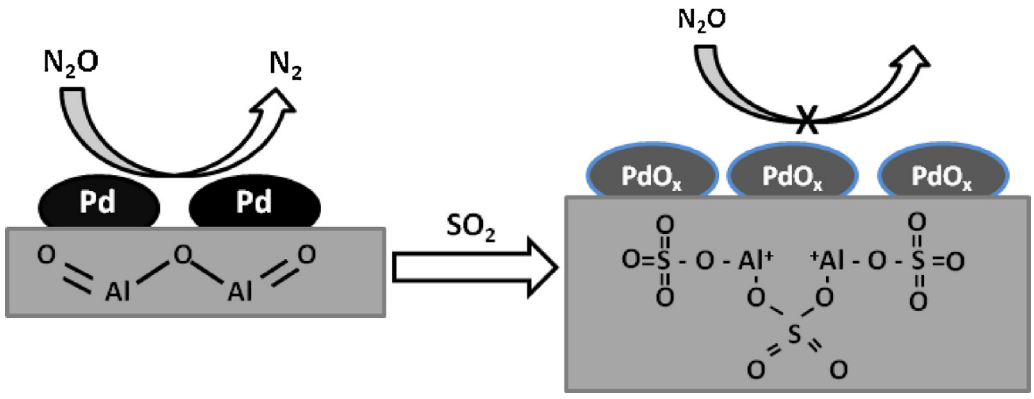

Fig. 9. Schematic illustration of SO_2 effects on de-N_2O process over Pd/Al_2O_3 catalysts.

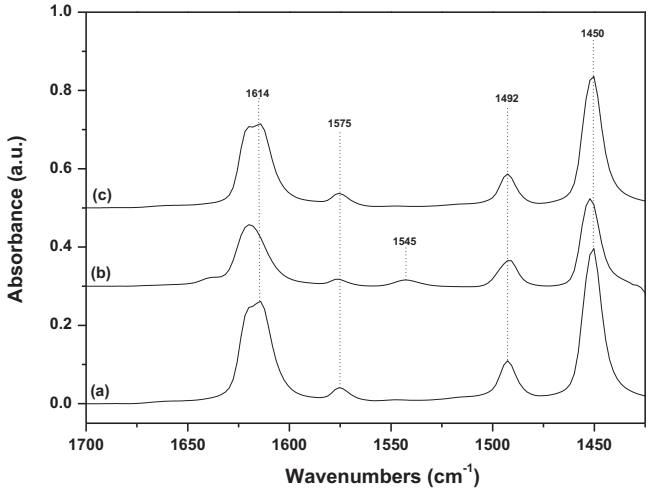

Fig. 11. DRIFTS spectra of fresh (a), SO_2-treated (b) and H_2O-treated (c) Pd/Al_2O_3 catalysts, following pyridine adsorption at 150 °C. Pretreatment conditions as in Fig. 7.

depicts the CO spectra obtained: before H_2O introduction (spectrum a), during $CO + H_2O$ co-adsorption (spectrum b) and after removal of H_2O from gas mixture (spectrum c). It is obvious that the interaction of H_2O molecules with the catalyst surface results in a significant decrease in intensity of carbonyl species bonded on Pd sites. This clearly demonstrates that H_2O simply competes with CO for the same active sites; the latter is fully confirmed from the complete restoration of CO band intensity after H_2O removal from feed stream (spectrum c). The catalytic results of Fig. 5 and the XPS data of Fig. 7 are consistent with this view.

It should be noted here that in the presence of water (spectrum b) several bands can be obtained in the hydroxyl stretching region attributed to diverse surface Al–OH groups. The bands in the 3800–3600 cm^{-1} region are attributed to different isolated hydroxyl species, whereas the features at *ca.* 3600–3500 cm^{-1} can be assigned to associated hydroxyl groups [40]. The low frequency bands at about 3450 cm^{-1} can be assigned to water molecules H-bonded to the acid sites of Al_2O_3 support [41].

The negative band at *ca.* 3736 cm^{-1} indicates that the CO adsorption in the presence of H_2O involves to some extent interactions with the less acidic hydroxyl groups of the sample. In this context, the overlapping bands at 1670–1600 cm^{-1} can be mainly assigned to bidentate carbonate and/or bicarbonate species formed through the interaction of CO with the hydroxyl groups [41].

3.5. FTIR spectroscopy of pyridine adsorption

To study the effect of SO_2 and H_2O on the acidic properties of Pd/Al_2O_3 catalysts, IR spectra of pyridine adsorption were acquired (Fig. 11) over fresh (spectrum a), SO_2-treated (spectrum b) and H_2O-treated (spectrum c) Pd/Al_2O_3 catalysts. Pyridine adsorption results in several well defined bands in the 1700–1400 cm^{-1} region attributed to pyridine species coordinated on both Brönsted and Lewis sites. Specifically, the bands at 1450 and 1614 cm^{-1} are assigned to pyridine coordinated on Lewis sites, the band at 1545 cm^{-1} to protonated pyridine on Brönsted sites, the band at 1492 cm^{-1} to pyridine on both Brönsted and Lewis sites, whereas that at 1575 cm^{-1} to physisorbed pyridine [42]. Among these bands those at 1450 and 1545 cm^{-1} are usually considered as most reliable for quantification of Lewis and Brönsted acid sites, respectively [42]. In Table 2 the concentration of acid sites (μmol/g) over Pd/Al_2O_3 catalysts, exposed to different pretreatment, is summarized. It is clear that the fresh Pd/Al_2O_3 catalyst demonstrates only

Table 2
Acidic properties of Pd/Al_2O_3 catalysts exposed to different pretreatment.

Catalyst sample	Brönsted acid sites (μmol/g)	Lewis acid sites (μmol/g)
Fresh	<1	115.5
SO_2-treated	17.3	158.4
H_2O-treated	<1	133.0

Lewis acid sites (spectrum a), in agreement with the surface acidity of Al_2O_3 supported catalysts [43]. However, SO_2 pretreatment results in a significant increase of Brönsted acid sites, followed by a moderate increase of Lewis acidity (spectrum b). Furthermore, a small shift toward higher frequency of the band at 1450 cm^{-1} for the SO_2 pretreated sample (Fig. 11; spectrum b) proclaims an increase in the Lewis acid sites strength [44]. These findings are in line with the XPS and DRIFTS data, implying the permanent effect of SO_2 on the acidity of Pd/Al_2O_3 catalysts. Similar literature IR studies of pyridine adsorption over metal oxides have clearly shown that SO_2 leads to the creation of Brönsted acid sites due to the formation of hydrogensulfite species [45].

In complete contrast, catalyst pretreatment with H_2O-containing mixtures does not result in any modification of Brönsted acidity, whereas a slight increase of Lewis acidity is obtained (Fig. 11; spectrum c). This indicates that H_2O, in contrast to SO_2, does not have any permanent effect on catalyst surface acidity, justifying the retrieval of de-N_2O efficiency after H_2O removal (Fig. 5).

3.6. Kinetic study

Table 3 summarizes the kinetic parameters, including the apparent activation energy (E_a) and the reactants partial reaction orders, for N_2O decomposition reaction under different feed compositions. In the case of direct N_2O decomposition the reaction obeys a first order dependence on N_2O with activation energy of ~31 kcal/mol. Addition of O_2 to the reaction mixture results in a first- and zero-order dependence on N_2O and O_2, respectively, whereas the E_a decreases to ~26 kcal/mol. The same kinetic behavior is observed when CH_4 is co-added with O_2 in N_2O stream; zero-order dependence on both O_2 and CH_4 with an activation energy of ~25 kcal/mol. The latter is in agreement with the negligible effect of both O_2 and CH_4 on N_2O conversion under oxidizing conditions (Fig. 1), verifying that the main pathway for N_2O elimination is its dissociation to N_2 and O(ad) even in the presence of reducing agents.

Addition of H_2O on the reaction mixture results in notable changes in the reaction mechanism including: (i) the first-order dependence on CH_4 and (ii) the negative-order dependence on H_2O (Table 3). This justifies the inhibiting effect of H_2O on the reaction rate as indeed observed in catalytic evaluation studies (Figs. 3, 5 and 6). On the basis of DRIFTS studies (Fig. 11) this inhibition was attributed to a competitive adsorption between water and reactants, in accordance to relevant literature studies [46–48]. A similar rate expression, *i.e.*, $r = k[CH_4]^1[O_2]^0[H_2O]^{-1}$, has been proposed for CH_4 oxidation over Pd/ZrO_2 [47]; according to the authors the inhibiting effect of water molecules can be ascribed to their tendency to compete with both vacancy and O_{ads} surface sites required for methane activation [47]. On the same basis, the hindering of CH_4 oxidation by water has been ascribed to the formation of inactive $Pd(OH)_2$ species [48]. Concerning the first-order dependence on CH_4, it could be argued that under H_2O excess conditions CH_4 has a key role in the N_2O elimination pathway, in contrast to its negligible effect under dry conditions. This beneficial effect of CH_4 can be possibly ascribed to its interaction with the $Pd(OH)_2$ species, rendering them active for N_2O adsorption/decomposition. However, further characterization studies are required to elucidate this point.

Table 3
Impact of feed composition on the kinetic parameters of de-N_2O reaction.

Power rate law: $r = k[N_2O]^a[O_2]^b[CH_4]^c[H_2O]^d[SO_2]^e$						
Feed composition	E_a (kcal/mol)	a	b	c	d	e
N_2O	30.8 ± 1.2[a]	0.99 ± 0.04	–	–	–	–
$N_2O + O_2$	26.1 ± 0.7	0.98 ± 0.07	0	–	–	–
$N_2O + O_2 + CH_4$	24.9 ± 0.8	0.95 ± 0.03	0	0	–	–
$N_2O + O_2 + CH_4 + H_2O$	22.6 ± 0.3	1.0 ± 0.03	0	1.1 ± 0.12	−1.5 ± 0.1	–
$N_2O + O_2 + CH_4 + SO_2$	36.8 ± 1.6	1.0 ± 0.03	0.32 ± 0.06	−0.18 ± 0.03	–	−0.38 ± 0.05

[a] Variances (±) in the kinetic parameters were estimated using the linear regression model with a confidence interval of 95%.

Finally, in the presence of SO_2 in the feed stream the reaction obeys a negative (−0.38) order dependence on SO_2, whereas the apparent activation energy increases to ~37 kcal/mol. The latter implies the detrimental influence of SO_2 on de-N_2O efficiency, as indeed observed in catalytic data (Figs. 2 and 6). This specific inhibition can be mainly interpreted based on XPS and DRIFTS studies, both indicating a poisoning of catalyst surface by sulfate compounds.

4. Conclusions

In the present study, the impact of SO_2 and H_2O molecules on the catalytic performance and surface characteristics of Pd/Al_2O_3 catalysts during N_2O decomposition in the presence of CH_4 and O_2 excess was demonstrated. Extensive catalytic, kinetic and surface chemistry studies revealed several important aspects concerning the effect of these molecules on catalyst surface chemistry and its correlation with the de-N_2O efficiency:

1. In the absence of O_2, the de-N_2O performance is notably improved by CH_4, due to the scavenging of strongly adsorbed O_{ads} by methane. However, under O_2 excess conditions, the beneficial effect of CH_4 is inferior.
2. H_2O has a detrimental influence on de-N_2O performance, which however is totally reversible due to its competitive adsorption on catalyst surface.
3. SO_2 addition in the feed stream results in an irreversible deactivation, ascribed to the creation of Brönsted acid sites on Al_2O_3 support; this in turn results, *via* metal–support interactions, to highly oxidized Pd species which are inactive for N_2O decomposition.
4. The electronic modifications induced by SO_2 over Pd sites are mainly attributed to the interactions of Pd sites with the sulfated Al_2O_3 support rather than to the direct interface of Pd sites with sulfur compounds.

Acknowledgments

Financial support by the program "THALIS" implemented within the framework of Education and Lifelong Learning Operational Programme, co-financed by the Hellenic Ministry of Education, Lifelong Learning and Religious Affairs and the European Social Fund is gratefully acknowledged. Authors wish also to thank the Laboratory of Surface Characterization at FORTH/ICE-HT in Patras, Greece, for performing the XPS measurements.

References

[1] J. Pérez-Ramírez, F. Kapteijn, K. Schöffel, J.A. Moulijn, Applied Catalysis B 44 (2003) 117.
[2] J. Pérez-Ramírez, Applied Catalysis B 70 (2007) 31.
[3] F. Kapteijn, J. Rodriquez-Mirasol, J.A. Moulijn, Applied Catalysis B 9 (1996) 25.
[4] D.J. Wuebbles, Science 326 (2009) 56.
[5] A.R. Ravishankara, J.S. Daniel, R.W. Portmann, Science 326 (2009) 123.
[6] J. Haber, M. Nattich, T. Machej, Applied Catalysis B 77 (2008) 278.
[7] S. Parres-Esclapez, M.J. Illán-Gómez, C. Salinas-Martínez de Lecea, A. Bueno-López, Applied Catalysis B 96 (2010) 370.
[8] S.C. Christoforou, E.A. Efthimiadis, I.A. Vasalos, Catalysis Letters 79 (2002) 137.
[9] V.G. Komvokis, G.E. Marnellos, I.A. Vasalos, K.S. Triantafyllidis, Applied Catalysis B 89 (2007) 626.
[10] G. Pekridis, C. Athanasiou, M. Konsolakis, I.V. Yentekakis, G.E. Marnellos, Topics in Catalysis 52 (2009) 1880.
[11] G. Pekridis, N. Kaklidis, M. Konsolakis, E. Iliopoulou, I.V. Yentekakis, G.E. Marnellos, Topics in Catalysis 54 (2011) 1135.
[12] G. Giecko, T. Borowiecki, W. Gac, J. Kruk, Catalysis Today 137 (2008) 403.
[13] E. Iwanek, K. Krawczyk, J. Petryk, J.W. Sobczak, Z. Kaszkur, Applied Catalysis B 106 (2011) 416.
[14] Li Xue, C. Zhang, H. He, Y. Teraoka, Applied Catalysis B 75 (2007) 167.
[15] N. Russo, D. Fino, G. Saracco, V. Specchia, Catalysis Today 119 (2007) 228.
[16] M.N. Debbagh, C. Salinas Martínez de Lecea, J. Pérez-Ramírez, Applied Catalysis B 70 (2007) 335.
[17] P.J. Smeets, M.H. Groothaert, R.M. van Teeffelen, H. Leeman, E.J.M. Hensen, R.A. Schoonheydt, Journal of Catalysis 245 (2007) 358.
[18] J.P. Dacquin, C. Lancelot, C. Dujardin, P. Da Costa, G. Djega-Mariadassou, P. Beaunier, S. Kaliaguine, S. Vaudreuil, S. Royer, P. Granger, Applied Catalysis B 91 (2009) 596.
[19] N. Russo, D. Mescia, D. Fino, G. Saracco, V. Specchia, Industrial and Engineering Chemistry Research 46 (2007) 4226.
[20] H. Cheng, Y. Huang, A. Wang, L. Li, X. Wang, T. Znang, Applied Catalysis B 89 (2009) 391.
[21] L. Obalová, K. Pacultová, J. Balabánová, K. Jirátová, Z. Bastl, M. Valášková, Z. Lacný, F. Kovanda, Catalysis Today 119 (2007) 233.
[22] J. Pérez-Ramírez, F. Kapteijn, Applied Catalysis B 47 (2004) 177.
[23] S. Kameoka, K. Kita, T. Takeda, S. Tanaka, S. Ito, K. Yuzaki, T. Miyadera, K. Kunimori, Catalysis Letters 69 (2000) 169.
[24] M. Konsolakis, C. Drosou, I.V. Yentekakis, Applied Catalysis B 123 (2012) 405.
[25] G. Corro, C. Cano, J.L.G. Fierro, Journal of Molecular Catalysis A 315 (2010) 35.
[26] S. Colussi, F. Arosio, T. Montanari, G. Busca, G. Groppi, A. Trovarelli, Catalysis Today 155 (2010) 59.
[27] P. Granger, P. Malfoy, P. Esteves, L. Leclercq, G. Leclercq, Journal of Catalysis 187 (1999) 321.
[28] M. Brun, A. Berthet, J.C. Betrolini, Journal of Electron Spectroscopy and Related Phenomena 104 (1999) 55.
[29] A.S. Ivanova, E.M. Slavinskaya, R.V. Gulyaev, V.I. Zaikovskii, O.A. Stonkus, I.G. Danilova, L.M. Plyasova, I.A. Polukhina, A.I. Boronin, Applied Catalysis B 97 (2010) 57.
[30] B. Mirkelamoglu, G. Karakas, Applied Catalysis A 299 (2006) 84.
[31] G. Corro, O.V. Cuchillo, F. Banuelos, J.L.G. Fierro, M. Azomoza, Catalysis Communications 8 (2007) 1977.
[32] L.F. Liotta, G.A. Martin, G. Deganello, Journal of Catalysis 164 (1996) 322.
[33] M.J. Kelly, J. Kim, G.W. Roberts, H.H. Lamb, Topics in Catalysis 49 (2008) 178.
[34] C.C. Chang, Journal of Catalysis 53 (1978) 374.
[35] A. Pieplu, O. Saur, J.C. Lavalley, M. Pijolat, O. Legendre, Journal of Catalysis 159 (1996) 394.
[36] T.C. Yu, H. Shaw, Applied Catalysis B 18 (1998) 105.
[37] A.I. Juez, A.M. Arias, M.F. García, Journal of Catalysis 221 (2004) 148.
[38] R.S. Monteiro, L.C. Dieguez, M. Schmal, Catalysis Today 65 (2001) 77.
[39] L. Zhang, D. Weng, B. Wang, X. Wu, Catalysis Communications 11 (2010) 1229.
[40] A. Martínez-Arias, M. Fernández-Garcia, A. Iglesias-Juez, J.A. Anderson, J.C. Conesa, J. Soria, Applied Catalysis B 28 (2000) 29.
[41] A.M. Turek, I.E. Wachs, E. DeCanio, Journal of Physical Chemistry 96 (1992) 5000.
[42] J.A. Lercher, A. Jentys, Studies in Surface Science and Catalysis 168 (2007) 435.
[43] H.H. Zhao, G.Y. Xie, Z.Y. Liu, Y.Z. Liu, Acta Chimica Sinica 66 (9) (2008) 1021.
[44] A. Travert, A. Vimont, A. Sahibed-Dine, M. Daturi, J.-C. Lavalley, Applied Catalysis A 307 (2006) 98.
[45] M. Ziolek, J. Kujawa, O. Saur, A. Aboulayt, J.C. Lavalley, Journal of Molecular Catalysis A: Chemical 112 (1996) 125.
[46] G. Pekridis, N. Kaklidis, V. Komvokis, C. Athanasiou, M. Konsolakis, I.V. Yentekakis, G.E. Marnellos, Journal of Physical Chemistry A 114 (2010) 3969.
[47] K. Fujimoto, F.H. Ribeiro, M. Avalos-Borja, E. Iglesia, Journal of Catalysis 179 (1998) 431.
[48] R. Burch, P.K. Loader, F.J. Urbano, Catalysis Today 27 (1996) 243.